Comparative Evaluation of MR-Based Partial-Volume Correction Schemes for PET

Carolyn Cidis Meltzer, Paul E. Kinahan, Phil J. Greer, Thomas E. Nichols, Claude Comtat, Michael N. Cantwell, Michael P. Lin and Julie C. Price

Departments of Radiology and Psychiatry, University of Pittsburgh, Pittsburgh, Pennsylvania

Because of limitations of spatial resolution, quantitative PET measurements of cerebral blood flow, glucose metabolism and neuroreceptor binding are influenced by partial-volume averaging among neighboring tissues with differing tracer concentrations. **Methods:** Two MR-based approaches to partial-volume correction of PET images were compared using simulations and a multicompartment phantom. The two-compartment method corrects PET data for the diluting effects of cerebrospinal fluid (CSF) spaces. The more complex three-compartment method also accounts for the effect of partial-volume averaging between gray and white matter. The effects of the most significant sources of error on MR-based partial-volume correction, including misregistration, resolution mismatch, segmentation errors and white matter heterogeneity, were evaluated. We also examined the relative usefulness of both approaches in PET studies of aging and neurodegenerative disease. **Results:** Although the three-compartment method was highly accurate (with 100% gray matter recovery achieved in simulations), it was also more sensitive to all errors tested, particularly image segmentation and PET-MR registration. **Conclusion:** Based on these data, we conclude that the two-compartment approach is better suited for comparative PET studies, whereas the three-compartment algorithm is capable of greater accuracy for absolute quantitative measures.

Key Words: emission tomography; MRI; aging; partial-volume correction; atrophy

J Nucl Med 1999; 40:2053–2065

The accuracy of in vivo measurements of tracer concentration in brain structures of interest is affected by several factors, particularly the relation between object size and scanner spatial resolution. Biases in the measured tracer uptake of small structures associated with resolution blurring are known as partial-volume errors (*1*). Despite substantial improvements in scanner resolution over the past decade, quantitative PET measurements of cerebral blood flow, glucose metabolism and neuroreceptor binding are still influenced by partial-volume averaging among neighboring tissues. Early work by Hoffman et al. (*1*) and Kessler et al. (*2*) used geometrically simple, high-contrast phantoms to estimate errors caused by partial-volume effects. These experiments, however, did not fully reflect the complexity of PET images of the human brain. Several investigators have since used simulated PET data to more closely approximate the impact of partial-volume effects on human PET studies (*3–8*). Underestimation of cortical activity associated with partial-volume averaging of gray matter with expanded cerebrospinal fluid (CSF) spaces has been shown to confound the comparison of subject groups with differing magnitudes and regional distributions of cerebral volume loss (*9,10*). Thus, partial-volume effects may affect especially the interpretation of PET studies of elderly populations or neurodegenerative disease.

The high-contrast, high-resolution anatomic detail available with MRI techniques has led to the development of MR-based methods to correct PET data for partial-volume effects. Several investigators have used MR determinations of total brain CSF volume to adjust whole-brain metabolic rates for age- or disease-related cerebral atrophy (*10,11*). Anatomically localized approaches to partial-volume correction were made possible by the development of reliable means to spatially register MR and PET images (*12,13*). Initially using prospective coplanar PET and MR image acquisition, Meltzer et al. (*4,14*) implemented a two-compartment approach to partial-volume correction of PET data that accounted for the influence of CSF on quantitation of regional brain PET data. A potential limitation of this method was the lack of correction for gray-white partial-volume averaging, which could affect the study of conditions in which the normal proportionality of gray to white matter may not be maintained (e.g., Alzheimer's disease) (*15,16*). A three-compartment modification of this method added a correction for partial-volume averaging between gray and white matter (*17*). In an alternate method, Rousset et al. (*5*) developed an MR-based partial-volume correction approach that incorporated anatomic information into the time-activity data from neuroreceptor PET studies and have shown accuracy similar to that of the three-compartment approach (*18*). Although the theoretic soundness of these methods has been reported, their relative sensitivity to error in actual PET studies has been addressed only partially (*3,18–21*).

The accuracy of MR-based partial-volume correction may be affected by several potential sources of error. The more

Received Dec. 14, 1998; revision accepted Apr. 19, 1999.

For correspondence or reprints contact: Carolyn Cidis Meltzer, MD, PET Facility, B-938, University of Pittsburgh Medical Center, 200 Lothrop St., Pittsburgh, PA 15213–2582.

significant of these are misregistration of the MR and PET datasets, inaccurate estimation of resolution effects, inaccurate segmentation of the MR image data into brain tissue components and potential heterogeneity of brain white matter. In their original forms, both the two-compartment and three-compartment methods were performed on a slice-by-slice basis and required coplanar acquisition of the MR and PET data. We have adapted these approaches to perform regional partial-volume correction of the total brain PET volume using retrospectively registered MR data. The goal of this work was to assess the relative impact of various sources of error associated with misregistration, resolution mismatch, segmentation errors and white matter heterogeneity on the two-compartment and three-compartment approaches to partial-volume correction. This comparison was conducted using PET simulations created from brain MR data and using PET and MR image data of a multicompartment phantom.

MATERIALS AND METHODS

Theory

The basic algorithms for the two- and three-compartment methods are briefly summarized here for later reference (*4,17*). The two-compartment method regards the observed PET image intensity, $I_O(x)$, as the convolution of the scanner point spread function, $h(x)$, with the sum of tracer distribution a brain tissue compartment, $I_T(x)$, and a CSF compartment, $I_C(x)$:

$$I_O(x) = (I_T(x) + I_C(x))***h(x), \qquad \text{Eq. 1}$$

where x is the three-dimensional position vector and *** represents the three-dimensional convolution operator. We can define a support function, or voxel map, for the location of brain tissue voxels as:

$$s_T(x) = \begin{cases} 1, & \text{if the voxel located at x contains brain tissue} \\ 0, & \text{otherwise.} \end{cases} \qquad \text{Eq. 2}$$

A similar definition for the support function of CSF voxels, $s_c(x)$, gives $s_T(x) + s_c(x) = 1$. The support functions can be determined from voxel-based segmentation of the MR image. In the CSF, the tracer concentration is assumed to be zero, so we can write:

$$I_O(x) = (I_T(x)s_T(x))***h(x). \qquad \text{Eq. 3}$$

If we further assume that the tissue concentration consists of small fluctuations about a larger mean value, then, to a good approximation:

$$I_O(x) \approx I_T(x)(s_T(x)***h(x)), \qquad \text{Eq. 4}$$

and we can estimate the true tissue tracer concentration as:

$$I_T(x) \approx \frac{I_O(x)}{s_T(x)***h(x)}. \qquad \text{Eq. 5}$$

Note that this is only valid for brain tissue voxels, that is, where $s_T(x) = 1$, and if the assumption of small fluctuations about a larger mean is met.

In the three-compartment model, we subdivide the brain tissue compartment into gray matter and white matter compartments such that $I_T(x) = I_G(x) + I_W(x)$, so that Equation 1 becomes:

$$I_O(x) = (I_G(x) + I_W(x) + I_C(x))***h(x). \qquad \text{Eq. 6}$$

The associated support functions now satisfy the relation $s_G(x) + s_W(x) + s_C(x) = 1$. If we again assume the CSF tracer concentration to be zero and further assume the white matter to be homogeneous with a constant tracer concentration c_W, Equation 6 can be rewritten as:

$$I_O(x) = (I_G(x)s_G(x) + c_W s_W(x))***h(x). \qquad \text{Eq. 7}$$

If we again assume that the gray matter concentration consists of small fluctuations about a larger mean value, then, similar to Equations 4 and 5, we have:

$$I_G(x) \approx \frac{I_O(x) - c_W(s_W(x)***h(x))}{s_G(x)***h(x)}. \qquad \text{Eq. 8}$$

Note that this is now valid only for gray matter voxels, that is where $s_G(x) = 1$.

Phantom Testing of Partial-Volume Correction Methods

Measurement of Point-Spread Function. The point-spread function was measured in both air and water for a Siemens 951R/31 tomograph (CTI PET Systems, Knoxville, TN), which has a 10.5-cm axial field of view, a plane thickness of 3.4 mm, a best-case in-plane resolution of 5.8 mm and a scatter fraction of ~10% when operated in two-dimensional mode (*22*). The measurement in water was performed to more closely approximate the point- spread function obtained in practice because measurements in air do not account for the broadening of the point-spread function associated with Compton scattering by surrounding tissue.

Point sources were made by soaking dry 1.5-mm-diameter beads in aqueous ^{18}F solution. They were then attached to 1.0-mm-diameter glass capillary tubes with cyanoacrylate glue and coated with a thin layer of cyanoacrylate glue to prevent leaching out of the absorbed ^{18}F solution. Separate sources were constructed for the air and water measurements with activities of $\sim 5 \times 10^6$ Bq (150 μCi). For this level of activity, scanner dead time and random coincidence rates were not significant.

For the air measurements, one glass support rod was attached horizontally to the end of the PET scanner patient bed. To measure the point-spread function in a scattering medium, two point sources were imaged simultaneously in an elliptical phantom filled with water, with one source radially centered and the other radially offset to 8.5 cm. For both sets of measurements, acquisitions were obtained in two-dimensional mode (septa in the field of view) at the locations described below, with approximately 10^6 coincidences collected at each position. Images were reconstructed using attenuation correction and our standard brain imaging parameters (no scatter correction, zoom of 2.0 and a Hamming apodization window cutoff at 0.8 of the Nyquist rate). The one exception was that the measurements in air were reconstructed without attenuation correction. The cutoff at 0.8 of the Nyquist rate is input into the scanner software as a cutoff of 0.4 and corresponds to a theoretic transverse resolution of approximately 7.3-mm full width at half maximum (FWHM). No axial smoothing was applied. For each reconstructed image, radial, tangential and axial profiles were extracted through the centroid of the resonstructed source positions and fitted with both Gaussian and Lorentzian functions, and the resulting FWHM of each fit was calculated. The goodness of fit in each case was determined by visual inspection.

For the air measurements, the point source was centered axially and positioned at radial positions of 0, 50 and 100 mm from the center of the field of view. For the measurements in water, 10 scans were acquired with the patient bed shifted axially into the scanner

by 1 mm between each acquisition, starting with the central point source centered axially in the field of view. The average measured FWHM values of the point sources in water were used to define a spatially invariant point-spread function, h(x), for partial-volume correction (Eqs. 5 and 8) of the phantom data described next.

Phantom Measurements. A standard 20-cm cylindric phantom (5300-mL volume) was fitted with two concentric plastic spheres that could be filled independently (Data Spectrum Inc., Raleigh, NC) (inner sphere: 3.5-cm diameter, 22-mL volume; outer sphere: 6.0-cm diameter, 70-mL volume). The sphere walls were 1 mm in thickness. The experimental arrangement is shown in Figure 1.

The chambers of the two spheres and the main phantom yielded three separate water-filled compartments to which ^{18}F was added to mimic the relative proportions of radioactivity among gray matter, white matter and CSF in blood flow or glucose metabolic PET images. Additionally, a gadolinium-based contrast agent for MR imaging was added to each compartment to approximate the relative contrast among gray matter, white matter and CSF in Tl-weighted MR images. The inner sphere or "white matter" compartment contained 2.7×10^{-5} MBq/mL ^{18}F and a 1:650 dilution of MR contrast agent, the outer sphere or "gray matter" contained 8.1×10^{-5} MBq/mL and a 1:65 dilution of MR contrast agent and the outer compartment or "CSF" component contained no ^{18}F or MR contrast agent. Aliquots of each of the solutions used in the gray matter and white matter compartments were reserved for measurement by a well counter to determine the calibration factor necessary to convert the scanner measurements to true radioactivity concentrations.

A 15-min emission scan of the phantom was acquired on the Siemens 951R/31 tomograph in two-dimensional mode with the nested spheres axially centered in the field of view, as indicated in Figure 1. Immediately after the emission scan, a standard 30-min transmission scan was acquired using rotating rods of ^{68}Ge-^{68}Ga. The phantom remained in the scanner for an additional 18 h to allow the ^{18}F to decay, after which a second 30-min transmission scan was acquired. The emission contaminated transmission scan was deliberately acquired for the sole purpose of PET-MR image alignment as decribed below. For quantitative results, the noncontaminated transmission scan was used for attenuation correction.

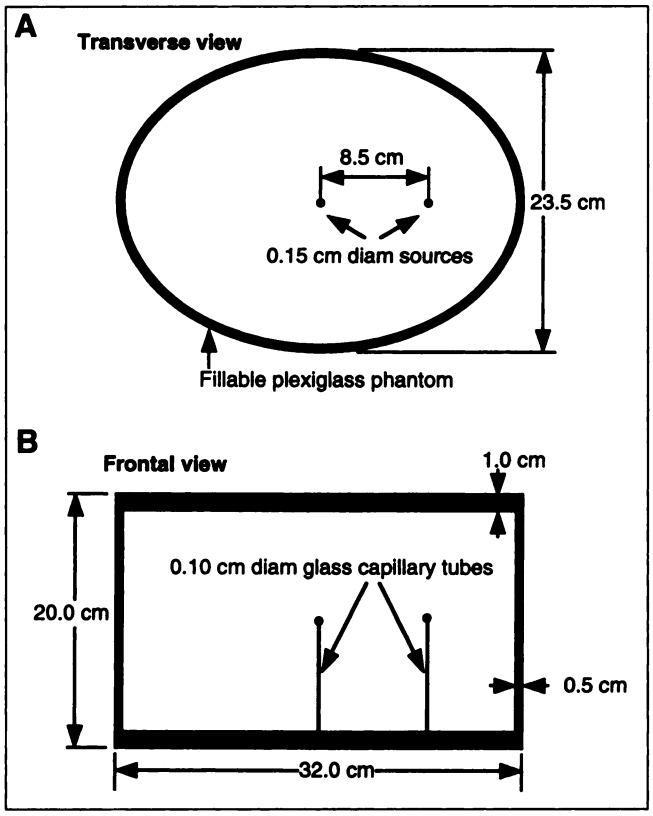

FIGURE 1. Transverse (A) and coronal (B) sections of phantom arrangement used to test partial-volume correction methods.

MRI of the phantom was performed 24 h after the second transmission scan on a 1.5-T Signa scanner (GE Medical Systems, Milwaukee, WI) using a standard head coil. A volumetric spoiled gradient recalled (SPGR) sequence (echo time = 5, repetition time = 25, flip angle = 40°; number of excitations = 1; 256 × 256 voxel matrix; voxel size = 0.94 × 0.94 × 1.50 mm^3) was obtained.

The PET scan of the phantom was reconstructed using the standard brain imaging parameters as described. Scatter correction was not performed; attenuation correction was based on the transmission scan. A phantom image reconstructed with the first transmission scan was used for alignment to the MR image. The MR and PET images of the phantom were coregistered by aligning the MR image to the PET image because the contamination of the transmission data by the emission activity resulted in clear visualization of all three phantom chambers. The alignment was performed manually using the iv_align software package (*23*). The accuracy of the alignment was estimated to be ±1 mm for all three linear coordinates and ±1 degree for all three rotational coordinates. After the alignment step, the MR data were segmented using manually applied thresholds, and both two-compartment (Eq. 5) and three-compartment (Eq. 8) partial-volume corrections were performed on the PET image reconstructed with the first transmission scan.

Simulation Studies

Simulation and Corrections of Partial-Volume Errors. SPGR MR brain images acquired in the coronal plane in young and elderly healthy subjects and Alzheimer's patients as part of ongoing research PET studies were used for simulations. To generate simulated PET image volumes, voxels in the MR image volumes corresponding to the calvarium, scalp and meninges were eliminated by hand tracing. The remaining brain volumes were then segmented into gray matter, white matter and CSF voxels by manually fitting corresponding signal intensity peaks to a Gaussian distribution (*17*). Voxel values were set to $c_G = 120$ (gray matter), $c_W = 40$ (white matter) and $c_C = 0$ (CSF). These relative values were selected to approximate normal uptake ratios among gray matter, white matter and CSF for the two most common tracers, [^{18}F]fluorodeoxyglucose and [^{15}O]water (*24*). Finally, simulated three-dimensional PET images were created, following Equation 7, by convolving the segmented MR image volumes with a Gaussian smoothing kernel over a range of resolution values (FWHM = 2–16 mm).

Correction Methods. For partial-volume correction of the simulated PET data using the two-compartment approach, the MR image was resegmented into brain tissue (including gray and white matter) and CSF voxel maps. The brain tissue concentration was then estimated using Equation 5. For the three-compartment method, the gray matter concentration was estimated by Equation 8 using $c_W = 40$.

For the simulated PET images corrected by the two- and three-compartment methods, the percentage mean gray matter

recovery (GMR) was calculated as:

$$GMR = 100\frac{\langle I_{T,G}(x), s_G(x)\rangle}{c_G\langle s_G(x), s_G(x)\rangle}, \quad \text{Eq. 9}$$

where c_G is the value assigned to gray matter during the simulation, the subscripts T (tissue) and G (gray matter) are for the true tissue uptake estimated by either the two- or three-compartment methods (Eq. 5 or 8). The notation $\langle\ \rangle$ is used for the standard three-dimensional inner product defined by:

$$\langle f(x), g(x)\rangle = \sum_{i=1}^{N} f(x_i)g(x_i), \quad \text{Eq. 10}$$

where there are N image voxels, and x_i is the location of image voxel I. The denominator in Equation 9 is thus simply the value assigned to gray matter (c_G) times the number of gray matter voxels ($\langle s_G(x), s_G(x)\rangle$). Note that GMR = 100% indicates perfect GMR (on average).

To compare the relative GMR in uncorrected and two- and three-compartment corrected images of a normal brain, simulated PET images were created from MR images acquired in a healthy 25-y-old man. The PET simulations were generated over a range of spatial resolutions (2- to 14-mm FWHM), and both the two-compartment and three-compartment partial-volume correction algorithms were applied.

Evaluation of Sources of Error. Simulations created from MR brain images acquired in a healthy 68-y-old woman were used to evaluate the relative impact of the following four sources of error on the two-compartment and three-compartment methods: resolution mismatch, white matter heterogeneity, segmentation errors and misregistration. For each evaluation, the following figures of merit were calculated: mean GMR (Eq. 9) and percent root mean square (RMS) error. The RMS figure of merit indicates the SD of individual voxels and was calculated for only the gray matter region as follows:

$$RMS = \frac{100}{c_G}\sqrt{\frac{\| s_G(x)I_{T,G}(x) - c_G s_G(x)\|^2}{\langle s_G(x), s_G(x)\rangle}}, \quad \text{Eq. 11}$$

where:

$$\| f(x)\|^2 = \langle f(x), f(x)\rangle. \quad \text{Eq. 12}$$

Resolution Mismatch. Because these MR-based correction methods depend on knowledge of the PET scanner resolution, the impact of a mismatch between true and estimated scanner resolution on the two-compartment and three-compartment methods was examined. This was accomplished by varying the FWHM of the point-spread functions, h(x), used to create the simulated PET images relative to that used for the partial-volume correction of Equations 5 and 8. Resolution mismatch between the two image datasets was examined over a range of values varying from 2 to 16-mm FWHM, in 2-mm increments.

White Matter Heterogeneity. Correction for partial-volume averaging between gray and white matter is an added feature of the three-compartment over the original two-compartment approach. To account for the diluting influence of white matter radioactivity on PET measurements, the three-compartment method requires the assumption that the white matter radioactivity has a homogeneous distribution. Therefore, to assess the influence of white matter heterogeneity (if present) on the two partial-volume correction schemes, a sinusoidal pattern of variation was introduced into the white matter compartment in the MR data, $I_W(x)$ (used in Equation 6), from which the PET simulations were created according to:

$$I_W(x) = c_W\left(1 + A\cos\left(\frac{2\pi x}{T}\right)\cos\left(\frac{2\pi y}{T}\right)\cos\left(\frac{2\pi z}{T}\right)\right), \quad \text{Eq. 13}$$

where x = (x,y,z) is the three-dimensional position vector, A is the amplitude of oscillation and T is the period (length) of the oscillations. This was tested using 12 different heterogeneity patterns by varying the amplitude and frequency of the sinusoidal pattern introduced into the white matter compartment (amplitudes = 5%, 10%, 20%, 50%; period = 2, 10, 50 voxels [voxel length 1 mm]) (Fig. 2). Simulated PET images were created at resolutions of 2- to 14-mm FWHM and both the two- and three-compartment corrections were applied.

Misregistration. In the computer simulations, the simulated PET and the tissue images were created from the same MR dataset and thus were perfectly coregistered. The Automated Image Registration (AIR) (University of California, Los Angeles, Los Angeles, CA) (*12*), which has been shown to be optimal relative to other existing registration methods (*13*), is an approach routinely used for registration of PET and MR image data in this laboratory and is associated with an alignment accuracy of <2.5 mm (*25*). However, the impact of small misregistration errors on the two- and three-compartment partial-volume corrections is unknown. To estimate the error associated with misregistration of actual PET and MR image data on the partial-volume correction algorithms, computer simulations were performed after introducing in-plane and z-axis misregistration of 1, 2 and 3 mm or 1 and 2 degrees between the simulated PET and MR tissue data. The AIR software was used to perform the misregistration and, for the angulation (pitch) differences, generated interpolated images.

Segmentation Error. The two-compartment method requires segmentation of MR image data into brain and CSF compartments, and the three-compartment method necessitates further identification of separate gray matter, white matter and CSF tissue components. The influence of misclassification of brain tissue voxels on partial-volume correction was assessed first by measuring the reproducibility of assigned signal intensity threshold values used for segmentation of the MR images. This was measured in brain MR data from 35 subjects (age 18–76 y) by repeating the selection of the intensity ranges over which the Gaussian distributions were fitted as described.

After estimating the variance of the calulated thresholds, the GMR and RMS figures of merit were recalculated for the two- and three-compartment methods after the CSF/gray matter and gray/white matter thresholds were shifted by ±1 and ±3 of the sample SDs as determined above.

Estimation of Errors in Practice. To estimate the combined effect of the four sources of error that could be reasonably expected in practice, a "reasonable" range for each error was defined, and global and regional figures of merit were calculated for all combinations. The global figures of merit were the GMR and RMS error as described. This was performed using MR images from a healthy 68-y-old woman as the basis for the simulation. The ranges for each error used were (a) resolution mismatch: (true [simulated PET], assumed) FWHM in mm = (6,8), (8,8), and (8,6); (b) white matter heterogeneity: period = 25 mm, amplitude = 0, 5% and 20% (Eq. 12); (c) misregistration: z-shift = 0, ±2 mm; pitch = 0, ±2° (for no z-shift only); (d) segmentation error: CSF/gray matter

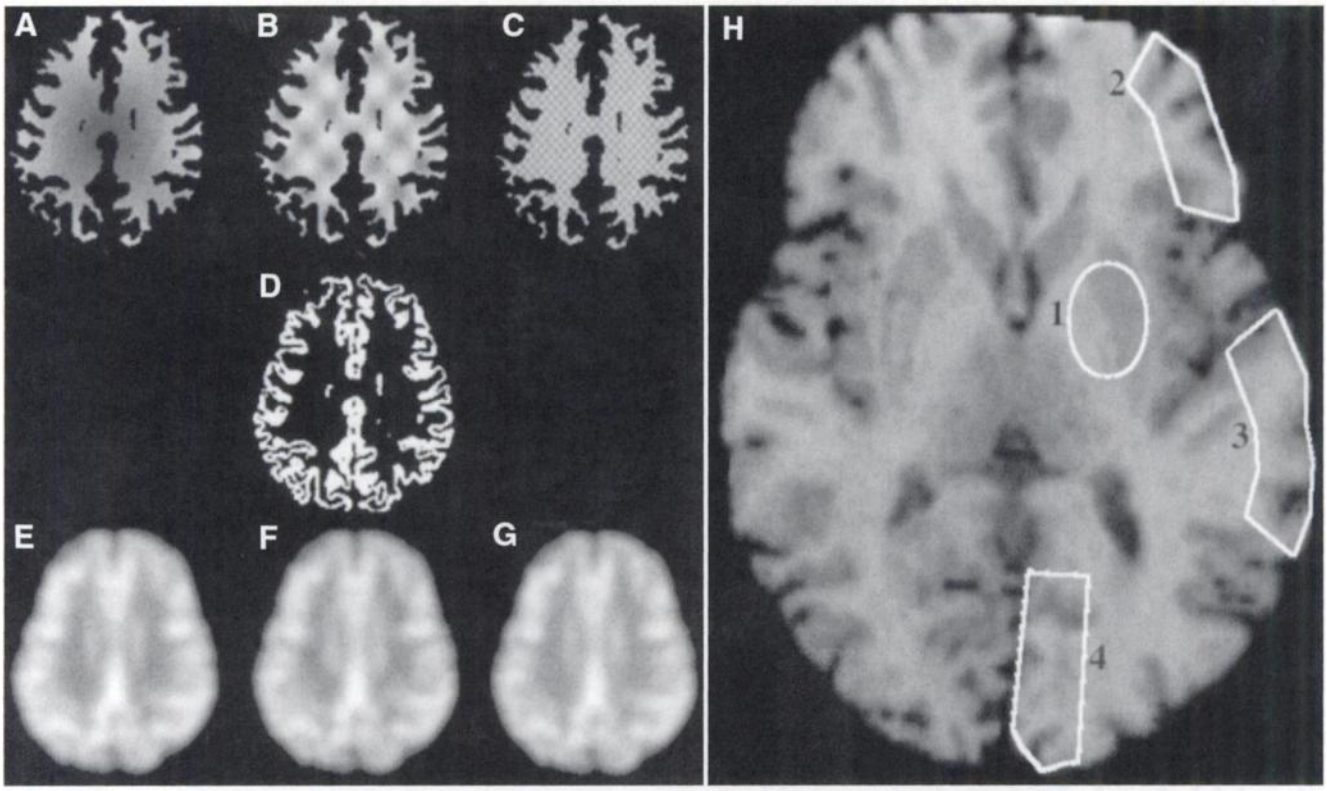

FIGURE 2. MR-based PET simulations. PET simulations of white matter heterogeneity (A–G): Segmented SPGR MR data show white matter compartment with sinusoidal patterns of ±50% variation in white matter pixel values at frequencies of 2 (A), 10 (B) and 50 (C). Segmented gray matter compartment in (D) was added to each white matter image (A, B and C) and composite image convolved with three-dimensional Gaussian smoothing kernel of FWHM = 8 mm to create corresponding simulated PET data (E, F and G, respectively). (H) ROI analysis of PET simulations. Axially reformatted SPGR MR image at level of basal ganglia illustrates localization of ROIs used in composite errors simulation experiment: 1, basal ganglia; 2, frontal cortex; 3, lateral temporal cortex; and 4, occipital cortex.

threshold shifted by 0, ±1 SD; gray/white matter thresholds shifted by 0, ±1 SD.

These complex perturbations consisted of combinations of errors, including three variations of resolution mismatch, three amplitude variations for the white matter inhomogeneity pattern, three z-axis misregistrations (0, +2 and −2 mm) plus three pitch variations that were performed only without z-axis shift, three variations in selection of the CSF/gray matter threshold and three variations in selection of the gray/white matter threshold. From these 405 combinations of errors, the average and SD of the GMR, RMS and region-of-interest (ROI) values were calculated. Four representative ROIs were drawn on the MR image and used to sample the corrected simulated data to estimate the impact of these errors on regional PET measurements in both cortical and deep brain structures for the two- and three-compartment correction methods (Fig. 2H).

Age- and Disease-Related Atrophy. To examine the importance of the additional white matter correction in the three-compartment method on PET studies of aging subjects and neurodegenerative disease, both correction methods were applied to PET simulations created from MR data acquired in 6 young, healthy individuals (age 18–38 y), 9 elderly subjects who were free of significant medical illness (age 59–79 y) and 5 subjects with Alzheimer's disease (age 65–74 y). The mean GMR for the uncorrected and corrected simulated PET images over a range of spatial resolution values (FWHM = 0–14 mm) were compared among the three subject groups. A Pearson correlation between age and GMR was calculated, and an unpaired *t* test was performed to assess the significance of uncorrected and corrected GMR differences between young and elderly healthy subjects.

RESULTS

Phantom Testing of Partial-Volume Correction Methods

Measurement of Point-Spread Function. By visual inspection, the transverse profiles of the point source in air were very closely approximated by a Gaussian function, whereas the axial profile was best fit with a 1/2(Gaussian) + 1/2(Lorenztian) function. The measured transverse resolution of the point sources in air varied from a FWHM of 6.8 mm at the center of the field of view to 7.4 mm at a radius of 10 cm, with an average of 7.2 mm. The average axial resolution was 3.5 mm, closely corresponding to the imaging plane thickness of 3.4 mm.

For the point sources in water, the transverse and axial profiles were very closely approximated by a Gaussian function. The measured transverse resolution of the point sources in water was 9.7-mm FWHM at the center of the field of view and 10.2 mm at a radius of 8.5 cm, with an average of 9.9 mm. The transverse resolution did not change significantly (<0.5 mm) with the axial position of the point

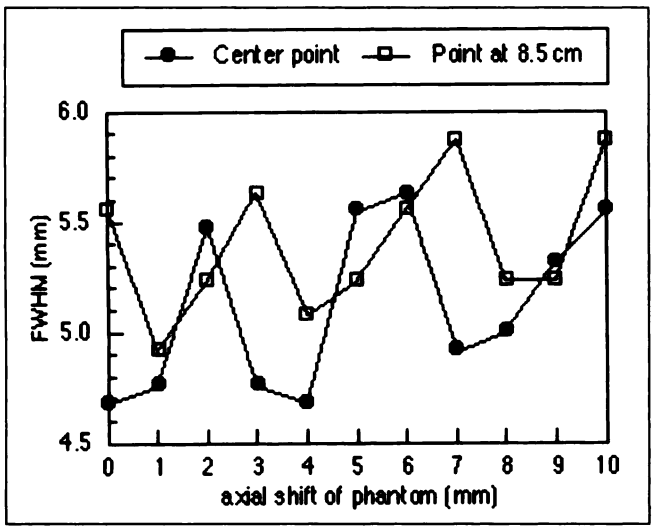

FIGURE 3. Axial resolution (full width at half maximum [FWHM]) as function of axial position for two point sources in water.

TABLE 1
Measured Activity in Inner Sphere (White Matter Compartment) and Outer Sphere (Gray Matter Compartment) of Test Phantom With and Without Corrections for Partial-Volume Effects

Method	White matter activity (MBq/mL)	Gray matter activity (MBq/mL)	GMR (%)
Well counter	1.5×10^{-5}	4.2×10^{-5}	NA
Uncorrected	2.3×10^{-5}	2.5×10^{-5}	58.2
Two-compartment correction	NA	3.2×10^{-5}	76.8
Three-compartment correction	NA	4.0×10^{-5}	95.8

GMR = ratio of PET measurement of gray matter activity and well counter measurement of activity in gray matter compartment; NA = not applicable.

sources. For the axial resolution of the point sources, Figure 3 shows the calculated axial resolution (FWHM) as a function of axial position. Note that the two points were axially offset by approximately 1 mm. The axial resolution of the point sources in water varied from a FWHM of 4.7 to 5.9 mm with an average of 5.3 mm. The apparent period of variation of the axial resolution was estimated by fitting sinusoids to the measured values and was approximately 3.7 mm, corresponding reasonably well with the scanning plane thickness of 3.4 mm. The average measured resolution values (transverse: 9.9-mm FWHM, axial: 5.3-mm FWHM) of the point sources in water were used to define the spatially invariant point-spread function, h(x).

Phantom Measurements. Figure 4 shows coronal sections through images of the test phantom corresponding to the coronal section shown in Figure 1. The average values for the gray matter regions shown in Figure 4 C and D are given in Table 1. The uncorrected gray matter compartment sampled from the phantom PET image measured only 58% of the well counter activity for the gray matter compartment. The GMR increased to 77% after two-compartment correction (Eq. 5) and 96% with application of the three-compartment correction (Eq. 8).

Simulation Studies

Simulation of Partial-Volume Errors and Corrections. The mean GMR in the uncorrected simulated PET data ranged from 59% to 81% over the range of resolutions tested. The two-compartment algorithm recovered 85%–99% of the assigned gray matter value, with the lower recovery values corresponding to relatively poorer resolutions. The percentage error in GMR in the uncorrected PET data was approximately halved by the two-compartment correction over the 2- to 14-mm FWHM range of resolutions (Fig. 5). As expected, the three-compartment correction resulted in full recovery of gray matter values at all resolution values.

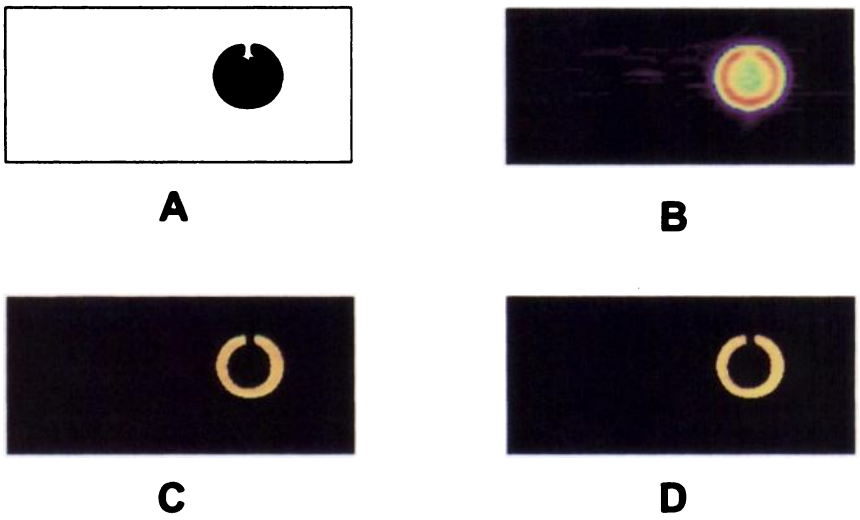

FIGURE 4. Coronal sections through images of test phantom. (A) Aligned MR image, (B) reconstructed PET image without partial-volume correction, (C) PET image with two-compartment correction, (D) PET image with three-compartment correction. Note that in (D) only region corresponding to gray matter is shown because Equations 5 and 8 are not valid outside this region. Each image display range is scaled to maximum for image.

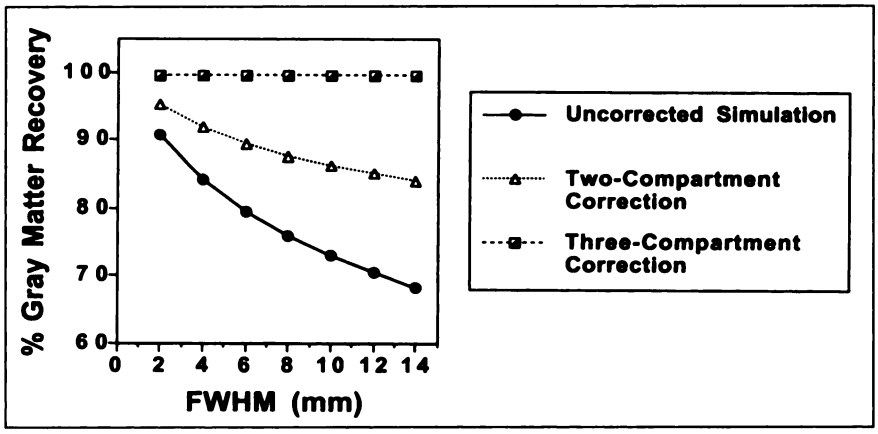

FIGURE 5. Simulated PET data created from MR data acquired in 25-y-old subject. Percentage GMR is plotted versus spatial resolution (full width at half maximum [FWHM] in mm) for uncorrected simulated PET and after two- and three-compartment partial-volume correction.

Evaluation of Sources of Error

Resolution Mismatch. The effects of resolution mismatch between the PET and convolved MR data were small (<10% error for ±2-mm FWHM) but relatively larger when scanner resolution (FWHM) was underestimated than when it was overestimated (Fig. 6).

White Matter Heterogeneity. There was a negligible influence of white matter heterogeneity on the two-compartment partial-volume–corrected GMR and RMS at all frequency and amplitude combinations and over all resolutions tested (Table 2, Fig. 7). The RMS error of the composite of gray matter voxels in the three-compartment corrected image data associated with introduction of white matter heterogeneity in the simulations ranged between 0% and 4.6%, with a negligible effect on average GMR (values ranging from 100.0% to 100.5%). An interaction between frequency of the sinusoidal white matter heterogeneity pattern and system resolution was observed, with a relatively smaller effect on GMR found at higher frequencies.

Misregistration. Small errors in registration between the MR and simulated PET image volumes resulted in larger RMS errors at relatively better spatial resolutions (Fig. 8). For example, at a FWHM of 2 mm, a 1-mm x-axis shift resulted in a 19.0% RMS error and a 4.6% reduction in GMR for the three-compartment correction, whereas at a FWHM of 12 mm and the same x-axis shift, the RMS error was 5.0% with only a 0.2% change in GMR. At poorer spatial resolutions, the impact of small shifts in image registration on the RMS error for the two-compartment correction was negligible. The RMS error introduced by the three-compartment correction nearly doubled at all resolutions when the magnitude of misregistration was increased from 1 to 2 mm, whereas the two-compartment correction was less sensitive to increasing misregistration (with a maximum increase in RMS error of 50% at 2-mm FWHM).

The effect of a change in angulation was similarly greater on the three-compartment than the two-compartment method. At a FWHM of 8 mm, a 1° difference in pitch between the coregistered MR and simulated PET images resulted in an RMS error of 24.6% (RMS = 24.7% with no tilt) and a GMR of 78.7% (GMR = 78.4% with no tilt) after two-compartment correction; an RMS error of 4.6% and a GMR of 99.3% were seen after three-compartment correction. At the same resolution and a 2° tilt, GMR was 78.3% and

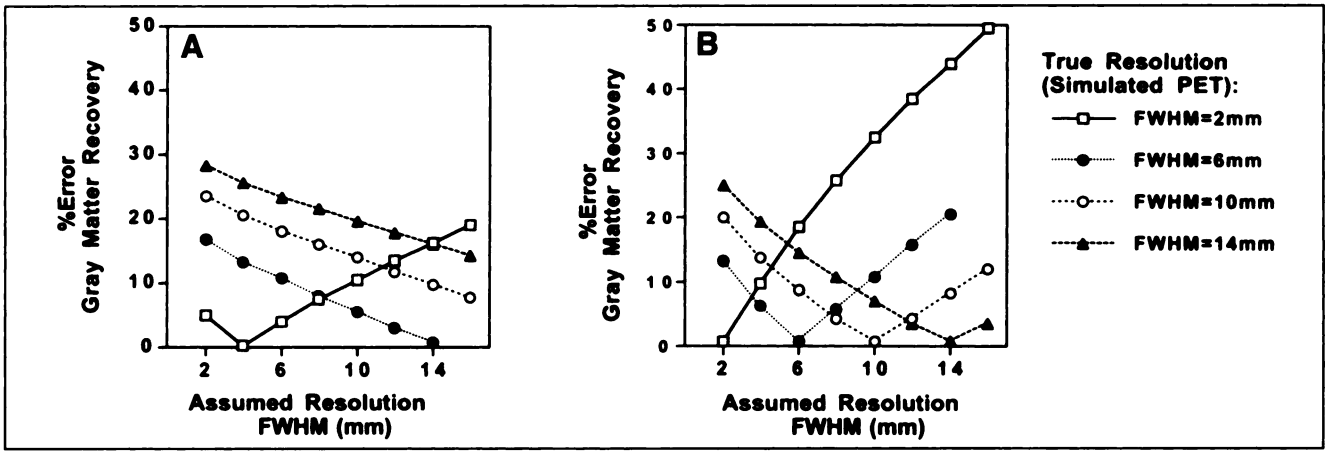

FIGURE 6. Simulated PET data show effect of mismatch in resolution between PET scanner and MR data on GMR for two-compartment (A) and three-compartment (B) correction methods. Increasing percentage error in total brain GMR is shown for larger discrepancies between two modalities. Note greater sensitivity of three-compartment method to resolution mismatch. (For clarity, all tested resolution values are not shown). FWHM = full width at half maximum.

TABLE 2
PET Simulations at FWHM = 8 mm: Effect of White Matter Heterogeneity on Two-Compartment and Three-Compartment Partial-Volume Correction Methods

White matter variation		RMS error (%)	
Frequency	Amplitude (%)	Two-compartment correction	Three-compartment correction
0	0	24.7	0.0
50	5	24.7	0.0
50	10	24.7	0.0
50	20	24.7	0.0
50	50	24.7	0.1
10	5	24.7	0.3
10	10	24.7	0.5
10	20	24.7	1.0
10	50	24.7	2.5
2	5	24.7	0.5
2	10	24.6	0.9
2	20	24.6	1.9
2	50	24.5	4.6

FWHM = full width at half maximum; RMS = root mean square.

98.7% and RMS was 25.3% and 8.7% for the two- and three-compartment correction methods, respectively.

Segmentation Error. The reproducibility of threshold selection for both the CSF/gray matter and gray matter/white matter segmentation was high. The mean difference (±SD) in the threshold selection repeated in a series of 35 brain MR images was 1.94% ± 2.40% (CSF/gray matter) and 0.49% ± 0.71% (gray matter/white matter).

The impacts of missegmentation of the brain and CSF compartments on the RMS error for the two- and three-compartment corrected simulated PET data are shown in Figure 9. The effect of altering the gray-white matter threshold on the three-compartment correction is also shown. Missegmentation of 1, 2 and 3 SDs in the brain-CSF threshold caused a negligible effect on the RMS error and GMR for the two-compartment correction. For the three-compartment correction, RMS errors of 1.3%–5.7%, and a slight overestimation of 101.1%–102.5% in mean GMR was observed with brain-CSF missegmentation. However, larger errors were encountered with missegmentation of the gray-white matter threshold, ranging from 4.1% to 11.1% in RMS error, with a mean GMR of 93.0%–96.8% over the resolutions tested (FWHM = 0–12 mm).

Estimation of Errors in Practice. The average GMR and RMS error over the 405 combinations are given in Table 3. The two-compartment method achieved an average GMR of 79% ± 1% with an average RMS error of 26% ± 1%, whereas for the three-compartment method the average GMR was 99% ± 2% and the average RMS error was 10% ± 5%. For each of these results the relatively small SD indicates that these are reasonable estimates of the average GMR and RMS error (Fig. 10). Four ROIs (Fig. 2H) were used to sample all 405 error simulations, and the average percentage regional gray matter recovery in the uncorrected and two- and three-compartment corrections is also given in Table 3. The two-compartment correction had the smallest effect on ROI 1, which is located in the basal ganglia and thus least influenced by the diluting effect of CSF. The three-compartment correction averages were within 4% of a perfect correction (i.e., 100% recovery) across all ROIs in the range of introduced errors.

Age- and Disease-Related Atrophy. The effect of age-related atrophy on GMR is illustrated in Figure 11. In the uncorrected data, an inverse relationship was observed between age and GMR (r^2 = 0.53). After applying the two-compartment and three-compartment corrections to the same data, this relationship is lost (r^2 = 0.17 and 0.0, respectively). Further, a significant difference in mean GMR was present between the young and elderly subjects in the uncorrected simulated PET data (P = 0.0001 in t test), with borderline significance maintained after application of the two-compartment partial-volume correction method (P = 0.03 in t test). Also, the two-compartment method corrected for most variance in GMR among young, elderly and

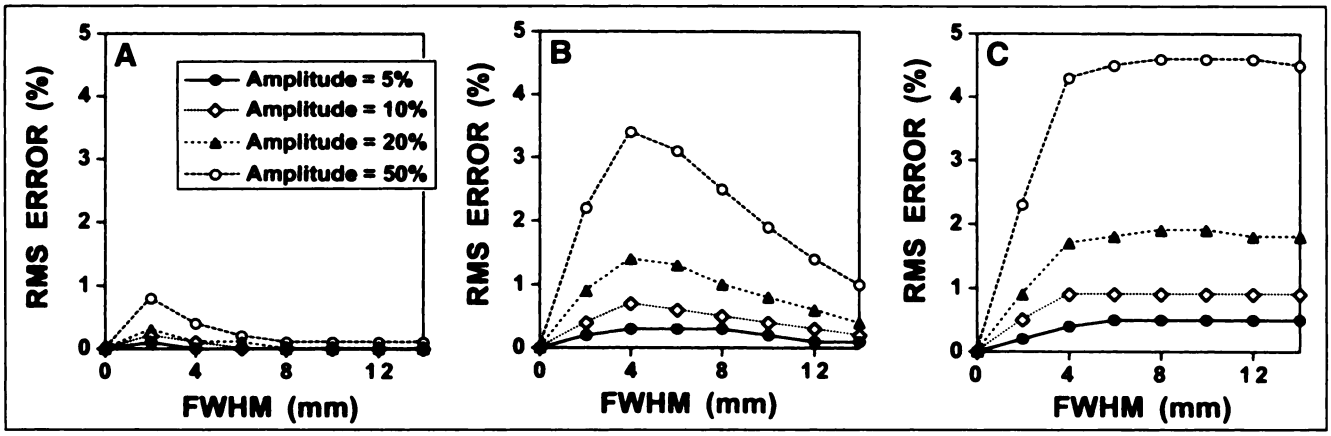

FIGURE 7. Graphs show influence of white matter heterogeneity on partial-volume correction of simulated PET data using three-compartment methods. Root mean square (RMS) error in GMR is plotted as function of amplitude of white matter variation over three frequencies of sinusoidal variation tested: 50 (A), 10 (B) and 2 (C). FWHM = full width at half maximum.

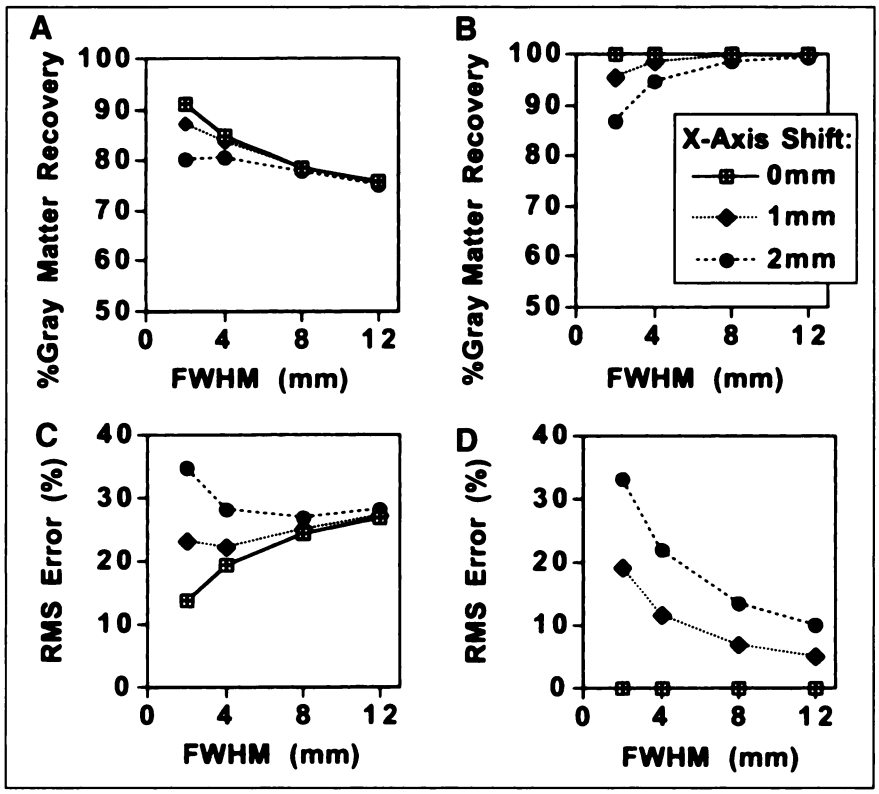

FIGURE 8. Effect of misregistration between PET and MR image volumes on two-compartment (A and C) and three-compartment (B and D) correction. Impact of 1- and 2-mm x-axis shift on percentage GMR (A and B) and root mean square (RMS) error (C and D) is shown. FWHM = full width at half maximum.

Alzheimer's disease groups as shown in Figure 11B and C. The uncorrected simulated PET data had lower uncorrected GMR values in the Alzheimer's disease subject group relative to the both young and elderly controls, and elderly normal values were lower than those of the young group (Fig. 11B and C). After two-compartment correction, the elderly and Alzheimer's GMR values were <1% of each other and within 5% of the values for the young at all resolution levels.

DISCUSSION

Age-related declines in regional cerebral blood flow, oxygen consumption and blood volume have been reported (*26–31*); however, these studies have not considered the potential influence of partial-volume effects caused by cerebral volume loss on regional PET measurements. Interestingly, the magnitude of the reported inverse correlations between age and these measures is similar to those shown in the uncorrected simulated PET data shown in Figure 11 (*30,31*). In these simulations, brain tracer concentration is held constant across the age range of subjects to quantify the partial-volume effects resulting from age-related changes in brain morphology inherent in the MR data. The relationship between age and GMR shown in the simulated PET data and its progressive deterioration with the two-compartment and three-compartment corrections

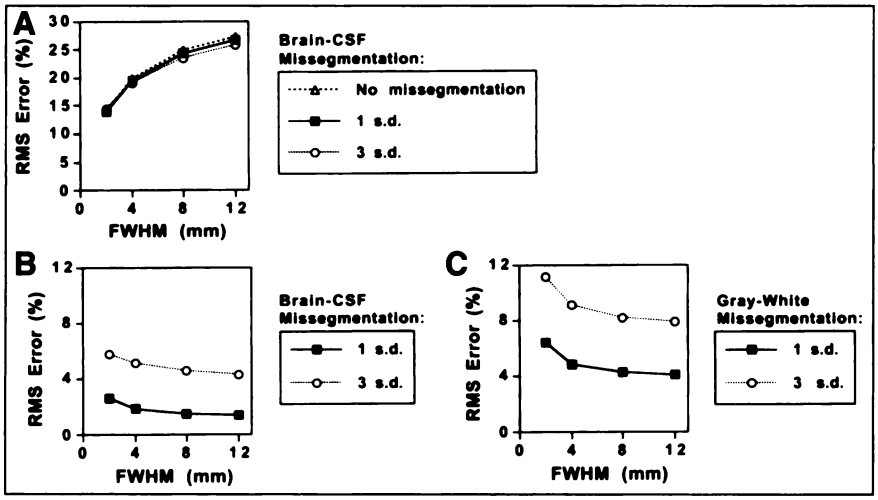

FIGURE 9. Effect of missegmentation on simulations over range of spatial resolutions. Root mean square (RMS) error with progressive missegmentation of MR image volume into brain and cerebrospinal fluid (CSF) compartments is plotted for two-compartment (A) and three-compartment (B) corrected data. RMS error resulting from missegmentation of gray matter and white matter compartments after three-compartment correction is shown in (C). FWHM = full width at half maximum.

TABLE 3
Results of Simulated Images with 405 Combinations of Sources of Error

	Uncorrected (%) (FWHM = 8 mm)	Two-compartment correction (%)	Three-compartment correction (%)
Average (total image) GMR and voxel RMS image			
GMR	60.2	78.7 ± 1.2	98.5 ± 2.0
RMS error	42.8	25.6 ± 1.4	10.2 ± 4.7
GMR for ROIs used in sampling			
ROI 1 (basal ganglia)	61.4	61.4 ± 1.3	103.4 ± 14.1
ROI 2 (frontal)	51.7	66.1 ± 8.0	99.2 ± 8.2
ROI 3 (temporal)	58.8	69.4 ± 4.7	101.6 ± 7.3
ROI 4 (occipital)	58.5	75.8 ± 3.5	101.2 ± 3.2

FWHM = full width at half maximum; GMR = gray matter recovery; RMS = root mean square; ROI = region of interest.

further illustrates the impact of cerebral atrophy associated with normal aging on physiologic PET measurements.

The two-compartment method is a simpler alternative to the three-compartment method but corrects brain PET data for only the dilutional effect of CSF. The three-compartment method has the advantage of also correcting for partial-volume averaging between gray and white matter. It requires additional assumptions, however, and is more sensitive to errors in segmentation, white matter heterogeneity and image registration accuracy. Segmentation error may be of particular practical concern because of the wide variety of segmentation approaches that may be used in MR-based partial-volume correction and the inherent difficulty in assessing the accuracy of segmentation in living human brain tissue. Another source of segmentation bias includes heterogeneity of the magnetic field, which is dependent on field strength and pulse sequence parameters and may vary from scanner to scanner. In addition, image contrast at ventricular-brain interfaces may be influenced by heterogeneity of CSF signal resulting from fluid motion. The overall relative practical value of the two MR-based partial-volume correction methods in PET studies of aging and neurodegenerative disease was assessed in simulated PET data from young and elderly healthy subjects and Alzheimer's patients (Fig. 11B and C). The purpose of these simulations was to determine if correcting for the dilutional effects of CSF alone was sufficient in PET studies of aging and neurodegenerative disease. If so, this would imply that the main confounding factor for group comparisons caused by cerebral atrophic changes accompanying normal aging and Alzheimer's disease was the relative increase in CSF spaces rather than a potential selective loss of gray matter. Indeed, the results of these simulations support the two-compartment method as a means of accounting for most partial-volume effect associated with between-group differences in cerebral brain volume.

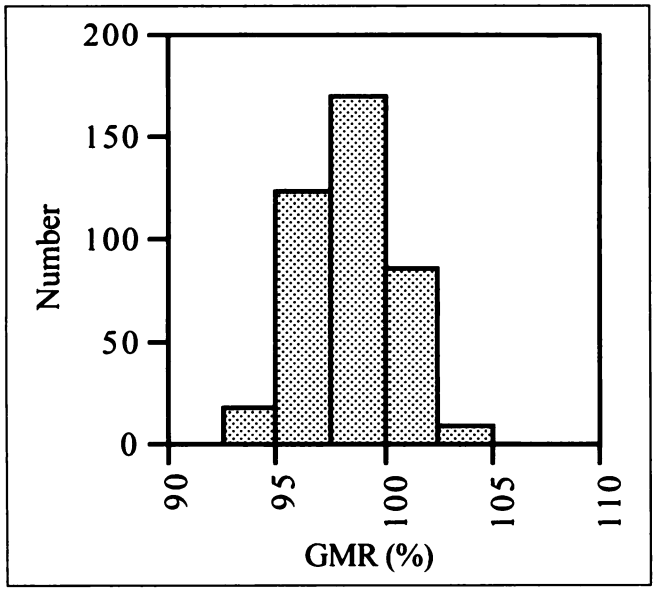

FIGURE 10. Histogram of gray matter recovery (GMR) for 405 combinations of variations in image alignment, resolution matching, segmentation and white matter heterogeneity. Mean, SD and range of figure of merit are given in Table 3.

The importance of homogeneity of white matter radioactivity for MR-based partial-volume correction was of particular interest in light of radiologic and pathologic evidence of white matter tissue alterations in normal aging and age-related neuropsychiatric disease (*32,33*). Although the magnitude of true variation in white matter radioactivity is unknown, Yamaji et al. (*34*) found approximately 5%–15% differences in PET measurements of mean white matter blood flow, oxygen extraction and blood volume between Alzheimer's patients with and without white matter lesions. Therefore, in the PET simulations, variations ranging from 5% to 50% were selected to test the potential impact of white matter heterogeneity on partial-volume correction of PET images. As expected, the RMS error of the composite of gray matter pixels associated with introduction of white matter heterogeneity was negligible when using the two-compartment partial-volume correction method. The three-compartment method, in which the white matter radioactivity concentration is estimated and subtracted from the PET data

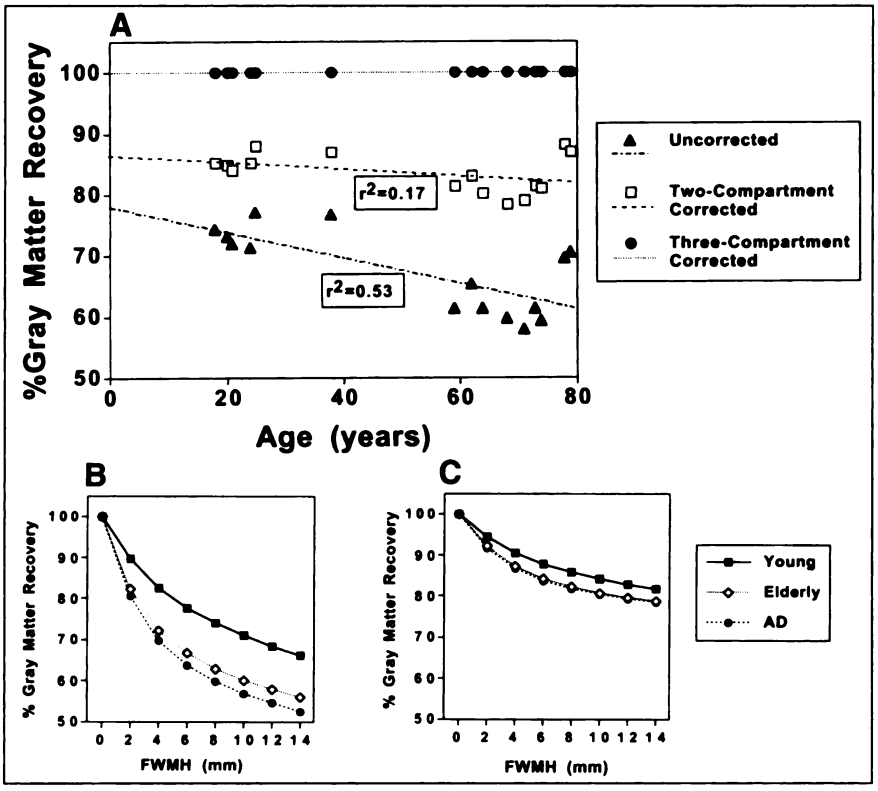

FIGURE 11. Impact of age and Alzheimer's disease (AD) on intersubject comparisons. (A) Graph shows effect of age on GMR in uncorrected, two-compartment corrected and three-compartment corrected simulated PET data at 8-mm FWHM (in-plane and z-axis). (B and C) Comparison of simulated PET data from young (n = 6), elderly (n = 9) and Alzheimer's disease (n = 5) subjects. Mean percentage GMR in each group over range of spatial resolutions (FWHM = 0–14 mm) is shown in uncorrected (B) and two-compartment-corrected (C) state.

to achieve a corrected gray matter tracer concentration, assumes that brain white matter is homogeneous. Thus, it was expected that the three-compartment method would be more sensitive to white matter heterogeneity. Although this was indeed true, the influence of white matter heterogeneity on the three-compartment correction was small. For example, with a 10% variation in white matter tracer concentration, errors of <1% in three-compartment-corrected gray matter values were attributed to the assumption of homogeneous white matter concentration. The error associated with white matter heterogeneity was minimized when the white matter variation was of high spatial frequency and low amplitude and when the system resolution was relatively poorer.

MR-based partial-volume correction approaches depend on accurate measurement of the true scanner resolution, which should be measured using point sources in water. On the PET scanner used, the average transverse resolution of point sources in air was 7.2 mm compared with 9.9 mm when measured in water. The point-spread function is nonstationary due to axial dependence (Fig. 3), but the variations in resolution across the field of view are somewhat reduced, likely because of the effect of Compton scatter. The results of the phantom measurements indicate that the residual spatial variance of the point-spread function appears to have a relatively small impact on MR-based partial-volume correction (Fig. 4). We note that the partial-volume correction methods of Equations 5 and 8 apply equally well to data measured in two- or three-dimensional mode (septa retracted), although the in vivo scanner resolution changes significantly in the three-dimensional mode (data not shown), and scatter correction likely would have to be applied to reduce bias to an acceptable level.

Both the two- and three-compartment methods showed sensitivity to a mismatch in spatial resolution between the simulated PET and the MR-derived brain tissue compartment images, although this effect was greater for the three-compartment correction (Fig. 6). The importance of convolving the MR tissue data to match the spatial resolution of the PET images was greatest at higher resolutions, whereas mismatches were better tolerated with poorer resolution data. For example, using the three-compartment method at a resolution mismatch of 2 mm between the simulated PET and MR tissue data resulted in a 9.8% error at a PET resolution of 2-mm FWHM and a 3.4% error at a PET resolution of 14-mm FWHM. It should be noted that at a theoretic high PET resolution of 2 mm, partial-volume averaging among tissues in the MR images should be considered. However, the purpose of the simulation was to show the effect of changing the PET resolution and so the resolution of MR was considered to be perfect. Because our scanner resolution, as measured by point sources in water, is 10 ± 1 mm across the field of view, the expected error associated with resolution mismatch would be <5% for both the two- and three-compartment approaches. For both methods, error was minimized if the MR tissue data were oversmoothed rather than undersmoothed; this effect was more important in the two-compartment correction because of the inherent undercorrection of gray matter. Investigating

the combinations of errors that could reasonably be expected in practice, the simulations indicated a best case ROI quantitative accuracy of ~80% ± 1% and an SD of ~25% for individual image voxels with the two-compartment method, whereas for the three-compartment method the ROI quantitative accuracy increased to ~98% ± 2% and the individual voxels SD dropped to ~10%. The experimental results indicate that these figures are slightly optimistic but show the same trend in comparing the two- and three-compartment methods.

CONCLUSION

Partial volume effects may confound PET studies of aging and neurodegenerative disease because of dilution of cortical signal by expanded CSF spaces and potential changes in white matter volume. We have shown in simulations and phantom studies the relative merit and response to error of two algorithms for MR-based partial-volume correction. Although the three-compartment approach to partial-volume correction is desirable in PET studies of subject groups in which the normal aging proportion of gray-to-white matter is altered, it is substantially more sensitive to small errors in missegmentation and PET-MR registration than the two-compartment approach. Minor additional error may be introduced by heterogeneity of brain white matter, which may be present in aging subjects. In practice, the three-compartment correction of phantom PET data yielded approximately 17% error in GMR, and complex simulations performed with a composite of "reasonable" sources of error showed an expected error of ~2%. Because the two-compartment method does not correct for the diluting effect of white matter on cortical signal, it has a higher overall error than the three-compartment method. However, it is relatively less sensitive to small errors that may affect intersubject comparisons and thus is more robust. We conclude that the greater precision afforded by the simpler two-compartment approach may make it better suited for comparative PET studies, whereas the three-compartment algorithm is capable of greater accuracy for absolute quantitative measures.

ACKNOWLEDGMENTS

This work was supported in part by U.S. Public Health Service grants MH01210 and MH52247 and by the Radiological Society of North America Research and Education Fund.

REFERENCES

1. Hoffman EJ, Huang SC, Phelps ME. Quantitation in positron emission computed tomography. 1. Effect of object size. *J Comput Assist Tomogr.* 1979;3:299–308.
2. Kessler RM, Ellis JR, Eden M. Analysis of emission tomographic scan data: limitations imposed by resolution and background. *J Comput Assist Tomogr.* 1984;8:514–522.
3. Meltzer C, Nichols T, Mintun M. Effect of resolution on recovery of gray matter activity in FDG PET [abstract]. *J Nucl Med.* 1995;36(suppl):114P.
4. Meltzer CC, Leal JP, Mayberg HS, Wagner HJ, Frost JJ. Correction of PET data for partial-volume effects in human cerebral cortex by MR imaging. *J Comput Assist Tomogr.* 1990;14:561–570.
5. Rousset O, Ma Y, Leger G, Gjedde A, Evans AC. Correction for partial-volume effects in PET using MRI-based 3D simulations of individual human brain metabolism. In: Meyers R, Cunningham V, Bailey D, Jones T, eds. *Quantification of Brain Function Using PET.* San Diego, CA: Academic Press; 1993:113–125.
6. Rousset O, Ma Y, Kamber M, Evans AC. 3D simulations of radiotracer uptake in deep nuclei of human brain. *Comput Med Imaging Graph.* 1993;17:373–379.
7. Videen TO, Perlmutter JS, Mintun MA, Raichle ME. Regional correction of positron emission tomography data for the effects of cerebral atrophy. *J Cereb Blood Flow Metab.* 1988;8:662–670.
8. Links J, Zubieta J, Meltzer C, Stumpf M, Frost J. Influence of heterogeneous background on "hot object" quantitation in brain emission computed tomography. *J Comput Assist Tomogr.* 1996;20:680–687.
9. Meltzer C, Zubieta J, Brandt J, Tune L, Mayberg H, Frost J. Regional hypometabolism in Alzheimer disease as measured by PET following correction for effects of partial-volume averaging. *Neurology.* 1996;47:454–461.
10. Tanna NK, Kohn MI, Horwich DN, et al. Analysis of brain and cerebrospinal fluid volumes with MR imaging: impact on PET data correction for atrophy. Part II. Aging and Alzheimer dementia. *Radiology.* 1991;178:123–130.
11. Alavi A, Newberg AB, Souder E, Berlin JA. Quantitative analysis of PET and MRI data in normal aging and Alzheimer's disease: atrophy weighted total brain metabolism and absolute whole brain metabolism as reliable discriminators. *J Nucl Med.* 1993;34:1681–1687.
12. Woods RP, Mazziotta JC, Cherry SR. MRI-PET registration with automated algorithm. *J Comput Assist Tomogr.* 1993;17:536–546.
13. Strother S, Anderson J, Xu X-L, Liow J, Bonar D, Rottenberg D. Quantitative comparisons of image registration techniques based on high-resolution of MRI of the brain. *J Comput Assist Tomogr.* 1994;18:954–962.
14. Meltzer CC, Bryan RN, Holcomb HH, et al. A method of anatomical localization for positron emission tomography using magnetic resonance imaging. *J Comput Assist Tomogr.* 1990;14:418–426.
15. Rusinek H, de Leon MJ, George AE, et al. Alzheimer disease: measuring loss of cerebral gray matter with MR imaging. *Radiology.* 1991;178:109–114.
16. Prohovnik I, Smith G, Sackeim HA, Mayeux R, Stern Y. Gray-matter degeneration in presenile Alzheimer's disease. *Ann Neurol.* 1989;25:117–124.
17. Mueller-Gaertner HW, Links JM, Prince JL, et al. Measurement of radiotracer concentration in brain gray matter using positron emission tomography: MRI-based correction for partial-volume effects. *J Cereb Blood Flow Metab.* 1992;12:571–583.
18. Rousset O, Ma Y, Evans AC. ROI- versus tissue-based partial-volume correction [abstract]. *Neuroimage.* 1997;5:B13.
19. Fahey F, Gage H, Harkness B. Accuracy of the Mueller-Gaertner partial-volume correction in brain PET [abstract]. *J Nucl Med.* 1996;37(suppl):225P.
20. Meltzer C, Zubieta J, Links J, Brakeman P, Stumpf M, Frost JJ. MR-based correction of brain PET measurements for heterogeneous gray matter radioactivity distribution. *J Cerebr Blood Flow Metab.* 1996;16:650–658.
21. Yang J, Huang S, Mega M, et al. Investigation of partial-volume correction methods for brain FDG PET studies. *IEEE Trans Nucl Sci.* 1996;43:3322–3327.
22. Barnes D, Egan G, O'Keefe G, Abbott, D. Characterization of dynamic 3-D PET imaging for functional brain mapping. *IEEE Trans Med Imaging.* 1997;16:261–269.
23. Michel, Christian. IV-align software package. Louvian-la-Neuve, Belgium: Catholic University of Louvain. Available at: http://www.topo.ucl.ac.be. Accessed October 19, 1999.
24. Mazziotta JC, Phelps ME, Plummer D, Kuhl DE. Quantitation in positron emission tomography: 5. Physical-anatomical effects. *J Comput Assist Tomogr.* 1981;5:734–743.
25. Wiseman M, Nichols T, Woods R, Sweeney J, Mintun M. Stereotaxic techniques comparing foci intensity and location of activation areas in the brain as obtained using positron emission tomography (PET) [abstract]. *J Nucl Med.* 1995;36(suppl):93P.
26. Kuhl D, Metter E, Riege W, Phelps M. Effects of human aging on patterns of local cerebral glucose utilization determined by the [^{18}F]fluorodeoxyglucose method. *J Cereb Blood Flow Metab.* 1982;2:163–171.
27. Loessner A, Alavi A, Lewandrowski K-U, Mozley D, Souder E, Gur R. Regional cerebral function determined by FDG-PET in healthy volunteers: normal patterns and changes with age. *J Nucl Med.* 1995;36:1141–1149.
28. Salmon E, Maquet P, Sadzot B, Degueldre C, Lemaire C, Franck G. Decrease of frontal metabolism demonstrated by positron emission tomography in a population of healthy elderly volunteers. *Acta Neurol Belg.* 1991;91:288–295.

29. Yoshii F, Barker W, Chang J, et al. Sensitivity of cerebral glucose metabolism to age, gender, brain volume, brain atrophy, and cerebrovascular risk factors. *J Cereb Blood Flow Metab.* 1988;8:654–661.
30. Marchal G, Rouix P, Petit-Taboue M-C, et al. Regional cerebral oxygen consumption, blood flow, and blood volume in healthy human aging. *Arch Neurol.* 1992;49:1013–1020.
31. Martin A, Friston K, Colebatch J, Frackowiak R. Decreases in regional cerebral blood flow with normal aging. *J Cereb Blood Flow Metab.* 1991;11:684–689.
32. Yue N, Arnold A, Longstreth W, et al. Sulcal, ventricular, and white matter changes at MR imaging in the aging brain: data from the Cardiovascular Health Study. *Radiology.* 1997;202:33–39.
33. Zubenko GS, Sullivan P, Nelson JP, Belle SH, Huff FJ, Wolf GL. Brain imaging abnormalities in mental disorders of late life. *Arch Neurol.* 1990;47:1107–1111.
34. Yamaji S, Ishii K, Sasaki M, et al. Changes in cerebral blood flow and oxygen metabolism related to magnetic resonance imaging white matter hyperintensities in Alzheimer's disease. *J Nucl Med.* 1997;38:1471–1474.